

# EEG-assisted retrospective motion correction for fMRI: E-REMCOR

Vadim Zotev<sup>\*</sup>, Han Yuan, Raquel Phillips, Jerzy Bodurka<sup>\*</sup>

Laureate Institute for Brain Research, 6655 S. Yale Avenue, Tulsa, OK 74136, USA

---

## Abstract

We propose a method for retrospective motion correction of fMRI data in simultaneous EEG-fMRI that employs the EEG array as a sensitive motion detector. EEG motion artifacts are used to generate motion regressors describing rotational head movements with millisecond temporal resolution. These regressors are employed for slice-specific motion correction of unprocessed fMRI data. The method does not require any specialized equipment beyond the standard EEG-fMRI instrumentation. Its performance is demonstrated by correction of fMRI data from four patients with major depressive disorder, who exhibited random head movements by 1–3 mm during a resting EEG-fMRI run. The fMRI datasets, corrected using eight EEG-based motion regressors, show significant improvements in temporal SNR (tSNR) of fMRI time series, particularly in the frontal brain regions and near the surface of the brain. The tSNR improvements are as high as 50% for large brain areas in single-subject analysis and as high as 25% when the results are averaged across the subjects. Simultaneous application of the EEG-based motion correction and physiological noise correction by means of RETROICOR leads to average tSNR enhancements as high as 35% for large brain regions. The proposed EEG-assisted method of retrospective fMRI motion correction (referred to as E-REMCOR) can be applied to improve quality of fMRI data with severe motion artifacts and reduce spurious correlations between the EEG and fMRI datasets caused by head movements.

*Keywords:* BOLD fMRI, EEG, EEG-fMRI, motion correction, motion artifacts

---

## 1. Introduction

Simultaneous EEG-fMRI, which combines the advantages of high spatial resolution of fMRI and high temporal resolution of EEG, has evolved into a powerful and widely used neuroimaging method (Mulert and Lemieux, 2010). However, both fMRI and concurrent EEG suffer from physiological confounds, particularly random head motions. Children, elderly people, patients with mental disorders (or other medical conditions), and even healthy controls engaged in demanding experimental tasks – can all exhibit significant head movements. The resulting motion artifacts, if not properly corrected, can severely reduce the quality of both fMRI and EEG data and even make the fMRI and EEG data sets unusable. Moreover, such artifacts can introduce spurious correlations between the fMRI and EEG time courses, potentially leading to incorrect interpretations of the multimodal neuroimaging data. Therefore, development of efficient motion correction techniques is particularly important for simultaneous EEG-fMRI.

The basic motion correction step in fMRI data processing is volume registration, which aligns each 3D multislice brain image (referred to as volume) in the fMRI time series with the reference brain image by means of a

rigid-body spatial transformation with six motion parameters (e.g. Friston et al., 1995; Jiang et al., 1995; Cox and Jesmanowicz, 1999). The volume registration alone cannot remove all motion artifacts in fMRI data for the following reasons: 1) head motions can cause spatially varying spin warping by changing spatial distributions of local magnetic susceptibility gradients (Jiang et al., 1995); 2) head motions can change spin excitation history, especially if they involve movements of tissue through the fMRI slice plane (Friston et al., 1996); 3) head motions, occurring on time scales shorter than the fMRI repetition time TR, can affect only some of the slices within a volume. These effects, together with fMRI signal variations due to cardiac and respiratory activity, make head movements appear non-rigid in fMRI images. The next common motion correction step is application of a linear regression procedure with the six motion parameters as regressors to reduce residual motion-related variations in fMRI time courses (e.g. Friston et al., 1996; Johnstone et al., 2006).

It has been long recognized that accurate motion detection and correction of high-resolution structural MRI and fMRI data, particularly in the widely used echo-planar imaging (EPI), requires motion regressors capable of describing head movements with high temporal resolution. Various approaches have been implemented to measure six rigid-body head motion parameters with fast temporal sampling independently of the volume registration. They include the use of navigator echoes (e.g. Fu et al., 1995;

---

<sup>\*</sup> Corresponding authors.

E-mail address: vzotev@laureateinstitute.org (V. Zotev);

jbodurka@laureateinstitute.org (J. Bodurka).

Welch et al., 2002), optical tracking devices (e.g. Tremblay et al., 2005; Zaitsev et al., 2006; Qin et al., 2009), or RF microcoils as active markers (e.g. Dumoulin et al., 1993; Ooi et al., 2011). These techniques can be used for both retrospective and real-time prospective motion correction (Ward et al., 2000). However, they all require a complex setup (e.g. specialized motion-sensitive equipment, hardware modifications to the MRI scanner) and/or specialized pulse sequences. They also have their shortcomings: the techniques based on navigator echoes or active markers increase the image acquisition time, while the optical tracking approaches require unobstructed lines of sight between the head and the tracking devices.

Another complication caused by random head movements in fMRI is that the effects of such movements are superimposed on the effects of physiological motions due to cardiac and respiratory processes. Large head movements can prevent accurate removal of cardiorespiratory artifacts by means of physiological noise correction methods such as RETROICOR (Glover et al., 2000). This method approximates the cardiorespiratory effects in fMRI time series by Fourier regressors depending on cardiac and respiratory phases. It has been suggested (Jones et al., 2008) that, in order to improve accuracy of the cardiorespiratory correction in the presence of random head motions, volume registration should be performed before the application of RETROICOR. The proposed motion-corrected version of RETROICOR (Jones et al., 2008), however, requires an individual set of regressors with different time courses for each voxel and can take into account only those random motion effects that are correctable by volume registration.

As with fMRI, head movements pose a major problem for EEG performed simultaneously with fMRI. Motion artifacts in EEG data, recorded inside an MRI scanner, appear because of the existence of conductive loops along the surface of the head due to electrical conductivity of the scalp between EEG electrodes. Rotational movements of such loops in the main magnetic field of the scanner induce artifact voltages picked up by EEG electrodes (see Methods below). Such artifact voltages exceed the EEG signals due to neuronal activity and overlap with essential frequency bands of the EEG spectrum, including the alpha band (8–13 Hz). Moreover, it has been shown that motion-related EEG artifacts, when convolved with the hemodynamic response function and correlated with fMRI time courses, predict plausible patterns of neuronal activation in the motor areas (Jansen et al., 2012).

Cardioballistic artifacts, caused by rapid head movements following the cardiac pulses, are quasiperiodic in time, and can be removed from the EEG data using techniques such as the average artifact subtraction method (Allen et al., 1998). Artifacts due to random head movements are more difficult to characterize and correct. Approaches have been proposed for real-time adaptive filtering of both

cardioballistic and random-motion artifacts using external motion monitoring by means of either a piezoelectric motion sensor (Bonmassar et al., 2002) or a special head cap with several wire loops (Masterton et al., 2007). Independent component analysis (ICA) (e.g. Bell and Sejnowski, 1995; Hyvärinen and Oja, 2000) is a powerful statistical method for separating signals from different sources in multichannel EEG recordings (e.g. Makeig et al., 1997). It has been successfully used to identify and remove various types of artifacts from EEG data in offline data analysis (e.g. Nakamura et al., 2006; Mantini et al., 2007).

Until the present, the motion correction efforts for fMRI and for EEG measured simultaneously with fMRI have followed two separate, though somewhat parallel, paths. No attempt has been made to combine the motion correction procedures developed separately for fMRI and EEG. Yet, the EEG array is itself a sensitive detector of head motions inside an MRI scanner, capable of tracking rapid head movements with millisecond temporal resolution.

Here we propose a novel EEG-based method for retrospective fMRI motion correction that uses motion artifacts in EEG data, recorded simultaneously with fMRI, to generate high-temporal-resolution motion regressors for fMRI. We refer to it as E-REMCOR (EEG-assisted RETrospective Motion CORrection). E-REMCOR does not require any specialized equipment beyond the standard EEG-fMRI instrumentation, and, importantly, can be applied retrospectively to any existing EEG-fMRI dataset. We demonstrate its efficiency in four patients with major depressive disorder (MDD), who exhibited random head movements by 1–3 mm during a nine-minute-long resting EEG-fMRI run.

## 2. Methods

### 2.1 E-REMCOR

The main reason for the appearance of artifacts in EEG data recorded inside an MRI scanner is the presence of an electrical (ionic) conductivity path between any pair of EEG electrodes. Because conductivity of the scalp tissue is about 20 times higher than that of the skull, it is sufficient to consider conductivity paths within the scalp, i.e. along the surface of the head. This is a simple model that captures the essential physics of the problem (Nakamura et al., 2006). An accurate electromagnetic analysis of EEG artifacts would require modeling several tissue layers with different electrical conductivities, including scalp, skull, CSF, and brain (e.g. Nunez and Srinivasan, 2006, chapters 4,6).

A change in magnetic flux penetrating a contour, formed by the conductive path together with EEG electrodes' leads, induces an electromotive force (EMF) in the contour, as described by Faraday law.

Because EEG signals are typically measured with respect to a single reference electrode (Ref), an effective contour for each EEG channel includes both that channel's electrode and Ref, but the contour's precise size and shape are unknown. If the EEG amplifier inputs draw no current, the voltage measured by a given EEG channel,  $V_{\text{EMF}}$ , is equal to the EMF itself. Rapidly changing magnetic fields due to RF pulses and switching gradients applied during an fMRI sequence produce MRI artifacts in the EEG data. Head motions in the scanner's main magnetic field, caused by cardiac pulsations, induce cardioballistic artifacts. Both types of artifacts are reasonably well understood and can be efficiently (though not completely) removed from EEG data acquired simultaneously with fMRI (e.g. Allen et al., 1998, 2000).

In this work, we focus on EEG artifacts resulting from random head motions in the static uniform magnetic field of the MRI scanner.  $V_{\text{EMF}}(t)$  refers to the voltage of such artifact measured by a given EEG channel. According to Faraday law,  $V_{\text{EMF}}(t) = -d\Phi/dt$ , so one can write:

$$\int_0^t V_{\text{EMF}}(\tau) d\tau = \Phi_0 - \Phi(t) = \Delta\Phi_R(t) + \Delta\Phi_D(t) \quad (1)$$

Here  $\Phi(t)$  is magnetic flux penetrating a given EEG channel's effective contour at time  $t$ , and  $\Phi_0$  is the flux at  $t=0$ . The term  $\Delta\Phi_R(t)$  describes the flux change due to rotations of the contour without deformations, while  $\Delta\Phi_D(t)$  accounts for possible small contour deformations in addition to rotations. Because the MRI scanner's main magnetic field (magnetic flux density)  $B_0$  is highly uniform, a parallel translation of a constant-geometry contour in any direction will not induce any EMF. For an arbitrary-shape contour of surface area  $A$ , the rotational part of the flux change can be expressed by a surface integral as follows:

$$\Delta\Phi_R(t) = B_0 \int_A \mathbf{n}_B \cdot [\mathbf{n}_0(s) - \mathbf{n}(s,t)] da_s \quad (2)$$

Here  $da_s$  is an elementary flat area (labeled by a variable  $s$ ) on the surface spanning the contour,  $\mathbf{n}(s,t)$  is a unit normal vector to this area at time  $t$ ,  $\mathbf{n}_0(s)$  is the normal vector at  $t=0$ ,  $\mathbf{n}_B$  is a unit vector along  $B_0$ , and “ $\cdot$ ” is dot product of two vectors.

In functional MRI, small rigid-body motions of the head are commonly described by six motion parameters defined in the image reference frame (Jiang et al., 1995). The first three parameters are translations along x (left-right), y (posterior-anterior), and z (inferior-superior) axes of the reference brain image. The other three parameters are rotations around x axis ( $\varphi$ , pitch), y axis ( $\psi$ , roll), and z axis ( $\theta$ , yaw). A general head rotation is described by the following 3D rotation matrix (Jiang et al., 1995), which is a product of three matrices,  $\mathbf{R}_x(\varphi)$ ,  $\mathbf{R}_y(\psi)$ ,  $\mathbf{R}_z(\theta)$ , corresponding to the three basic rotations:

$$\mathbf{R}(\varphi, \psi, \theta) = \mathbf{R}_z(\theta(t)) \cdot \mathbf{R}_x(\varphi(t)) \cdot \mathbf{R}_y(\psi(t)) \quad (3)$$

With the assumptions that the effective contour rotates rigidly with the head and that the reference brain image corresponds to  $t=0$ , Eq (2) can be re-written using the rotation matrix  $\mathbf{R}$  and the identity matrix  $\mathbf{I}$ :

$$\Delta\Phi_R(t) = B_0 \mathbf{n}_B \cdot [\mathbf{I} - \mathbf{R}(\varphi, \psi, \theta)] \int_A \mathbf{n}_0(s) da_s \quad (4)$$

The last expression shows that the temporal change in magnetic flux,  $\Delta\Phi_R(t)$ , which can be determined from the EEG motion artifact according to Eq (1), is, in general, a function of all three fMRI rotational motion parameters. If  $\mathbf{n}_B$  is collinear with the image z axis, the flux change will only depend on  $\varphi$  and  $\psi$ . This is a consequence of the fact that rotation of any vector around  $B_0$  (by angle  $\theta$ , yaw) does not change its projection on  $B_0$ . For small rotation angles, a power series expansion of  $\mathbf{R}(\varphi, \psi, \theta)$  to the lowest (first) order in  $\varphi$ ,  $\psi$ , and  $\theta$  yields the following linear approximation with constants  $c_1$ ,  $c_2$ , and  $c_3$  depending on  $A$ ,  $B_0$ , and the vectors  $\mathbf{n}_0(s)$  and  $\mathbf{n}_B$  in the image reference frame:

$$\Delta\Phi_R(t) \approx c_1\varphi(t) + c_2\psi(t) + c_3\theta(t), \quad \varphi, \psi, \theta \ll 1 \quad (5)$$

Equations (4) and (5) suggest that, if geometrical properties of three different contours and their orientations at  $t=0$  are known precisely, the rotational motion parameters  $\varphi(t)$ ,  $\psi(t)$ , and  $\theta(t)$  can be accurately determined for any  $t$  using simultaneous measurements of  $\Delta\Phi_R(t)$  functions for those three contours. For motion artifacts, recorded by different EEG channels, the effective contour properties are unknown. Nevertheless, if motion artifacts dominate the EEG recordings,  $\Delta\Phi_R(t)$  functions, obtained according to Eq (1), can be used as motion regressors, because they represent different linear combinations of the actual motion parameters. Selection of EEG channels for generation of such regressors is rather ambiguous, however.

For the purpose of motion correction (to be conducted after the removal of MRI and cardioballistic artifacts), it is important to separate EEG artifacts arising due to random head motions,  $V_{\text{EMF}}(t)$ , from other instrumental and physiological artifacts present in EEG recordings, as well as from signals related to the actual neuronal activity. The instrumental artifacts may include, for example, residual MRI artifacts, EEG amplifier baseline drifts, signals due to mechanical vibrations, and interference signals picked up by EEG electrodes with poor electrical connections to the scalp. The physiological artifacts include eye blinking effects and residual cardioballistic signals. As mentioned in the introduction, ICA makes it possible to separate signals from different sources in multichannel EEG recordings. Using ICA, signals  $V_i(t)$  from  $N$  EEG channels can be approximated by linear combinations of  $M$  non-Gaussian independent components (ICs)  $F_j(t)$ :

$$V_i(t) = \sum_{j=1}^M b_{ij} F_j(t) + \varepsilon_i(t), \quad i = 1 \dots N, M \leq N \quad (6)$$

Here,  $b_{ij}$  are elements of the matrix  $\mathbf{W}^{-1}$  (the inverse of the unmixing matrix  $\mathbf{W}$ ), describing projections of the found independent components  $\{F_j\}$  back onto the EEG electrode space (e.g. Bell and Sejnowski, 1995; Makeig et al., 1997). The quantity  $\varepsilon_i(t)$  is an error term also including the  $i$ th-channel's Gaussian noise. In the present work, the ICA is performed on the EEG data after the removal of both MRI and cardioballistic artifacts. The ICA decomposition, Eq (6), makes it possible to select a subset  $\{F_k\}$  of the independent components, consisting of those ICs ( $k=1 \dots K$ ) that correspond to EEG artifacts caused by random head motions, so that

$$V_{\text{EMF}}^{(i)}(t) \approx \sum_{k=1}^K b_{ik} F_k(t), \quad i = 1 \dots N, K \leq M \leq N \quad (7)$$

The motion-related ICs are identified in the present study according to the following three main criteria. *First*, the ICs of interest should reflect all major motion effects, observed in the EEG data, and exhibit high degrees of non-Gaussianity, as measured by the ICs' kurtosis or negentropy (Hyvärinen and Oja, 2000). The effects of rapid head movements are usually clearly visible both in the EEG recordings and in the IC time courses. *Second*, the relevant ICs should not be attributable to other known artifact sources such as eye blinking or cardioballistic effects. *Third*, the ICs of interest should have approximately bipolar topographies. An IC topography is a spatial map corresponding to a column of the  $\mathbf{W}^{-1}$  matrix and describing projections of a given IC onto the EEG electrodes. A "bipolar" IC topography is defined here as the one that provides significant (i.e. exceeding a sufficiently high magnitude threshold) signal contributions, which exhibit opposite polarities for EEG channels on two opposite sides of the EEG array. Such bipolar topographies have routinely appeared in our ICA-based studies of both cardioballistic artifacts and EEG artifacts due to random head motions. We hypothesize that they reflect simple head rotations, i.e. rotations around a fixed axis passing through the head. The IC waveform in this case can be interpreted as time dependence of the angular speed of rotation (of unknown sign and amplitude) around such axis. Bipolar scalp topographies of EEG motion artifacts have been mentioned in the work by Jansen et al., 2012, but those authors based their arguments on a physically unrealistic model of the head as a uniformly conductive sphere (Yan et al., 2010).

The term  $\Delta\Phi_D(t)$  in Eq (1) describes magnetic flux changes due to deformations of the effective contour. Such deformations result primarily from changes in pressure exerted on the EEG electrodes and their leads by the padding underneath and on both sides of the head during head movements. Unlike  $\Delta\Phi_R(t)$ , the term  $\Delta\Phi_D(t)$

may depend on both rotational and translational motion parameters. The corresponding IC topographies may show contributions to EEG motion artifacts in parietal, occipital, and temporal regions. In the present study, we focus on the rotational effects, and neglect the deformational term  $\Delta\Phi_D(t)$  for the sake of simplicity.

Comparison of Eqs (1), (5), and (7) suggests that time integrals of motion-related ICs can be used as motion regressors corresponding to different linear combinations of the rotational motion parameters. We use each IC from Eq (7) (with  $k=1 \dots K$ , where  $K$  is the total number of ICs describing random head motions) to generate two separate motion regressors as follows:

$$\int_0^t F_k(\tau) d\tau = \int_{t-\Delta t}^t F_k(\tau) d\tau + \int_0^{t-\Delta t} F_k(\tau) d\tau = R_1^{(k)}(t) + R_2^{(k)}(t) \quad (8)$$

Here,  $\Delta t$  is a short constant time interval, and the integration limit  $t-\Delta t$  is set to 0 for  $t < \Delta t$ . This definition of regressors provides more flexibility in describing both short-term and long-term motion effects. The IC-based regressors will not approximate any linear trends that may be present in the actual motion parameters  $\varphi(t)$ ,  $\psi(t)$ , and  $\theta(t)$ , because any constant voltage offsets are removed during EEG data acquisition, and all ICs have zero means. This is not a limitation for fMRI motion correction, however, because any linear trend in fMRI time series is explicitly modeled as a nuisance effect and removed during fMRI data analysis.

The motion regressors  $R_1^{(k)}(t)$  and  $R_2^{(k)}(t)$ , defined in Eq (8), have the same temporal sampling as the EEG recordings. For correction of motion effects in fMRI data, these regressors need to be sub-sampled to match acquisition times  $\{t_s\}$  for each slice in the fMRI dataset (after the steady state is reached). Motion correction is then performed for each fMRI voxel time series using the following linear regression procedure:

$$S_{\text{fMRI}}(t_s) = \beta_0 + \beta_1 R_L(t_s) + \sum_{k=1}^K [\beta_{k1} R_1^{(k)}(t_s) + \beta_{k2} R_2^{(k)}(t_s)] + \varepsilon(t_s) \quad (9)$$

Here,  $\{\beta\}$  are fit coefficients for each 3D voxel, and  $R_L(t_s)$  is a zero-mean linear regressor. Subtraction of the fit terms containing the  $R_1^{(k)}(t)$  and  $R_2^{(k)}(t)$  regressors from the original fMRI time series for each voxel yields a motion-corrected fMRI dataset. The effects of such motion correction on fMRI data can be evaluated by comparing temporal signal-to-noise ratio (tSNR) values before and after the correction. The tSNR is defined as follows:

$$\text{tSNR} = \text{mean}(S_{\text{fMRI}}(t_s)) / \text{std}(S_{\text{fMRI}}(t_s)) \quad (10)$$

It is an important characteristic of fMRI time courses and depends on fMRI acquisition parameters, tissue type, and the amount of physiological noise (Bodurka et al., 2007).

The proposed method, E-REMCOR, makes it possible to generate motion regressors capable of describing rotational head motions with much finer, millisecond temporal resolution. It can improve efficiency of fMRI motion correction by providing a more accurate approximation of the effects of rapid head movements occurring on time scales shorter than the repetition time  $TR$ . It can be applied simultaneously with RETROICOR and other methods for fMRI physiological noise correction utilizing slice-time information.

## 2.2 Experimental procedure

The study was conducted at the Laureate Institute for Brain Research. The research protocol was approved by the Western Institutional Review Board (IRB). Four unmedicated MDD patients (mean age  $33.5 \pm 12.5$  years, two females) participated in the study. All the participants provided written informed consent as approved by the IRB. The experimental protocol included real-time fMRI neurofeedback training runs as well as resting fMRI runs (Zotev et al., 2011). EEG recordings were performed simultaneously with fMRI. Only resting-state EEG-fMRI results (one run per subject) are reported in this paper. For the resting run, the participants were instructed not to move, but to relax and rest while looking at the fixation cross on the screen. No subject reported any discomfort resulting from wearing an EEG cap during the experiment.

All functional and structural MR images were acquired using a General Electric Discovery MR750 whole-body 3 Tesla MRI scanner with a standard 8-channel receive-only head coil array. A single-shot gradient-recalled EPI sequence with Sensitivity Encoding (SENSE, Pruessmann et al., 1999) was employed for fMRI. To enable accurate correction of MRI artifacts in EEG data, acquired simultaneously with fMRI, the EPI sequence was custom-modified to ensure that the repetition time  $TR$  was exactly 2000 ms (with 1  $\mu$ s accuracy). The following EPI imaging parameters were used: FOV=240 mm, slice thickness=2.9 mm, slice gap=0.5 mm, 34 axial slices per volume,  $96 \times 96$  acquisition matrix, echo time  $TE=30$  ms, SENSE acceleration factor  $R=2$ , flip angle=90°, sampling bandwidth=250 kHz. The fMRI run time was 8 min 40 s. Three EPI volumes (6 s) were added at the beginning of the run to allow the fMRI signal to reach steady state, and were excluded from data analysis. The EPI images were reconstructed into a  $128 \times 128$  matrix, so the resulting fMRI voxel size was  $1.875 \times 1.875 \times 2.9$  mm<sup>3</sup>. Physiological pulse oximetry and respiration waveforms were recorded (with 20 ms sampling interval) simultaneously with fMRI. A photoplethysmograph, placed on the subject's finger, was used for pulse oximetry, and a pneumatic respiration belt was used for respiration measurements. A T1-weighted magnetization-prepared rapid gradient-

echo (MPRAGE) sequence with SENSE was used to provide an anatomical reference for the fMRI analysis. It had the following parameters: FOV=240 mm, 128 axial slices per slab, slice thickness=1.2 mm,  $256 \times 256$  image matrix,  $TR/TE=5.0/1.9$  ms, acceleration factor  $R=2$ , flip angle=10°, delay time  $TD=1400$  ms, inversion time  $TI=725$  ms, sampling bandwidth=31.2 kHz, scan time=4 min 58 sec.

The EEG recordings were performed simultaneously with fMRI using a 32-channel MR-compatible EEG system from Brain Products GmbH. Each subject wore an MR-compatible EEG cap (BrainCap MR from EASYCAP GmbH) throughout the experiment. The cap is fitted with 31 EEG electrodes, arranged according to the international 10-20 system, and includes one ECG electrode placed on the subject's back. The EEG amplifier (BrainAmp MR plus) was positioned just outside the MRI scanner bore near the axis of the magnet approximately 1 m away from the subject's head. The amplifier was connected to the PC interface outside the scanner room via a fiber optic cable. The EEG system's clock was synchronized with the 10 MHz MRI scanner's clock using Brain Products' SyncBox device. The EEG signal acquisition was performed with 16-bit 5 kS/s sampling providing 0.2 ms temporal and 0.1  $\mu$ V measurement resolution. The EEG signals with the standard reference (FCz as Ref) were hardware-filtered during the acquisition in the frequency band between 0.016 Hz (10 s time constant) and 250 Hz. The electrical cables connecting the EEG cap to the amplifier were fixed in place using sandbags. To reduce head motions, two foam pads were inserted in the MRI head coil on both sides of the subject's head. Consistency of the padding's firmness across multiple subjects could not be ensured, however. The EEG data acquisition was monitored in real time using Brain Products' RecView software, which enabled online correction of MRI and cardioballistic artifacts.

## 2.3 Data analysis

Processing of the EEG data, acquired simultaneously with fMRI, was performed using Brain Products' Analyzer 2 software. Removal of the MRI and cardioballistic artifacts was based on the average artifact subtraction method. The MRI artifact template was defined using the MRI slice markers, output by the scanner and recorded during the EEG acquisition. The slice markers were also used to select a 520-second-long EEG data interval, precisely corresponding to the fMRI time series of 260 volumes. After the MRI artifact removal, the EEG data were downsampled to 250 S/s sampling rate (4 ms sampling interval) and low-pass filtered at 40 Hz (48 dB/octave). The cardioballistic artifact template was determined from the cardiac waveform recorded by the ECG electrode, and the artifact to be subtracted was defined by a

moving average over 21 cardiac periods. It should be noted that no high-pass filtering was applied to the EEG data beyond that performed during the EEG data acquisition.

Application of E-REMCOR includes three steps: i) independent component analysis of the EEG data; ii) integration of the components corresponding to major head motions; iii) correction of the fMRI dataset using the EEG-based motion regressors. In the present study, we used the FastICA algorithm (Hyvärinen, 1999), implemented in Analyzer 2. The ICA was applied to the EEG data from  $N=31$  channels over the entire measurement time interval, and the number of ICs was set to  $M=20$ . The ICs corresponding to random head motions, Eq (7), were then identified as described above. The number  $K$  of such ICs depends on the complexity of the subject's head movements, as well as performance of the ICA algorithm. In this work, we used the same  $K=4$  in each single-subject analysis to enable direct comparison and averaging of the results across the subjects. If more than four ICs satisfied the above-mentioned criteria, the four ICs characterized by the largest kurtosis values were selected. Time courses of the four selected ICs were exported from Analyzer 2 and integrated in MATLAB to generate two motion regressors,  $R_1^{(k)}(t)$  and  $R_2^{(k)}(t)$ , for each IC as defined in Eq (8), using  $\Delta t=0.4$  s. Mean values of these functions were subtracted, and magnitudes of the resulting waveforms were scaled to fit the  $[-1,+1]$  interval.

Analysis of the fMRI data was performed in AFNI (Cox, 1996; Cox and Hyde, 1997). The linear regression procedure, Eq (9), was implemented using 3dTfitter program, which makes it possible to apply individual regressors to the time course of any voxel. On the image level, each regressor in Eq (9) was represented by an AFNI 3D+time dataset with an individual time course for each slice determined by sub-sampling the regressor's time series to match acquisition times for that slice in the original fMRI dataset. The least-squares solution of Eq (9) by means of 3dTfitter program yielded the coefficients  $\{\beta\}$  as 3D datasets. Motion correction was carried out by subtracting the eight terms, corresponding to the  $R_1^{(k)}(t)$  and  $R_2^{(k)}(t)$  regressors in Eq (9), from the original fMRI dataset. Motion effects in both the original and corrected fMRI data were further evaluated using 3dvolreg program in AFNI. This program performs brain volume registration and slice timing correction. It provides estimates of the six fMRI motion parameters and computes the maximum displacement in the brain automask for each fMRI volume.

To evaluate simultaneous performance of E-REMCOR and RETROICOR, we carried out a separate fMRI data correction, in which eight RETROICOR regressors were added to the right-hand side of Eq (9). They included four cardiac regressors, defined as

$\cos(m\varphi_c)$  and  $\sin(m\varphi_c)$  with  $m=1,2$ , and four respiratory regressors, defined as  $\cos(m\varphi_r)$  and  $\sin(m\varphi_r)$  with  $m=1,2$ . Here,  $\varphi_c(t)$  is the cardiac phase and  $\varphi_r(t)$  is the respiratory phase, determined from the physiological recordings simultaneous with fMRI (Glover et al., 2000). Similar to the motion regressors, each RETROICOR regressor was represented by a 3D+time dataset with an individual time course for each slice obtained by the sub-sampling procedure based on the slice-time information.

### 3. Results

All four MDD patients, referred to as Subjects A, B, C, and D, exhibited significant head movements during the resting EEG-fMRI run. For these subjects, the maximum displacements in brain automasks over the entire run, computed for the original fMRI data, were found to be A) 2.2 mm; B) 3.0 mm; C) 1.8 mm; and D) 2.0 mm. After linear de-trending of the original fMRI datasets, the maximum displacements were A) 2.2 mm; B) 1.2 mm; C) 1.7 mm; and D) 1.2 mm. Therefore, each of the four subjects moved by at least 1 mm during the resting run.

Figure 1 illustrates identification of the ICs reflecting major random head motions in the ICA decomposition of the EEG data for Subject A. Both ICs' time courses (20 s time interval, left) and the corresponding topographies (right) are shown. This subject exhibited significant movements during the time interval spanning several fMRI volumes, with the most drastic motion occurring during the second half of the data acquisition for volume 61. The fMRI volumes are numbered 1 through 260. The four ICs ( $K=4$  out of total  $M=20$ ) in Fig. 1 are highly non-Gaussian (kurtosis values 251, 204, 26, and 16, respectively) and have bipolar topographies. Application of the same ICA procedure to the cardioballistic artifacts, subtracted previously from the EEG data using the average artifact subtraction method, also yielded several main cardioballistic ICs with bipolar topographies, but their kurtosis values were below 11. The topography of IC 1 in Fig. 1 is very similar to that of the cardioballistic IC (not shown) describing the pitch-like head rotation (i.e. rotation around the left-right axis) following the cardiac R peak. This similarity suggests that IC 1 also describes a pitch-like head rotation (the interhemispheric asymmetry of both topographies indicates an uneven placement of the EEG cap and/or uneven positioning of the head within the scanner). Indeed, examination of the six fMRI motion parameters shows that two parameters have the largest peak values at volume 61: the inferior-superior displacement (1.2 mm) and the pitch rotation (0.7 deg). Therefore, the most drastic head motion during the acquisition of volume 61 is the motion through the EPI slice plane. Such through-plane motions are known to

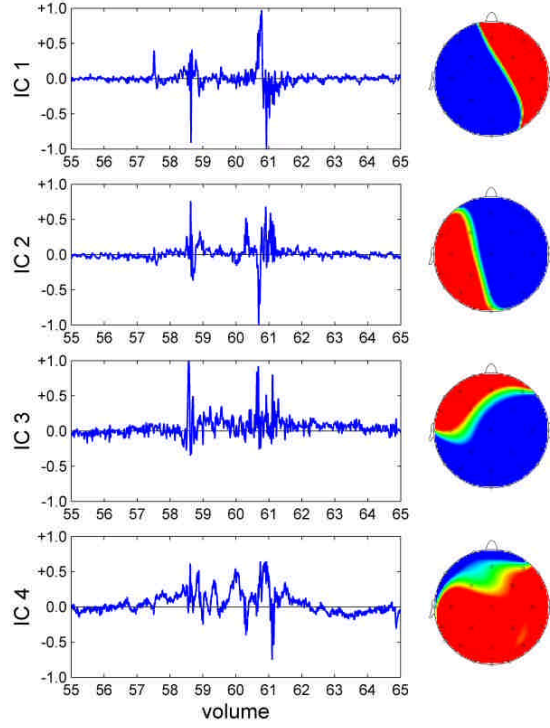


**Fig. 1.** EEG independent components reflecting major head motions of a single subject (Subject A). Both time courses (on the left) and the corresponding topographies (on the right) are shown. Temporal resolution is 4 ms. Each tick label along the time axis marks the end of data acquisition for a corresponding fMRI volume ( $TR=2$  s).

produce severe artifacts in fMRI data (Friston et al., 1996). The main independent component (IC 1 in Fig. 1) describes the pitch rotation as part of this motion.

Figure 2 exhibits time courses of eight motion regressors ( $R_1^{(k)}(t)$  in red,  $R_2^{(k)}(t)$  in blue,  $k=1\dots 4$ ) obtained by time integration of the four ICs in Fig. 1 (Subject A). The integration was performed as described in Methods section, and the regressors were scaled to fit the  $[-1, +1]$  interval. Note that all eight regressors in Fig. 2 reflect the significant head motions in the time interval around volume 61. The most drastic movement is particularly evident in the time courses of the  $R_1(t)$  and  $R_2(t)$  regressors based on IC 1, which both have sharp peaks in that interval. The regressors in Fig. 2 show small contributions from residual cardioballistic artifacts, which is not surprising, because, as discussed above for the case of IC 1, the same type of head rotation can contribute to both cardioballistic and random head motions.

Results of the E-REMCOR-based motion correction of the original fMRI data for Subject A are shown in Fig. 3. The correction was performed using 3dTfitter program as described in Methods section. The effects of such correction were evaluated by comparing tSNR values of each 3D voxel's time series before and after the correction. All acquired axial EPI slices are

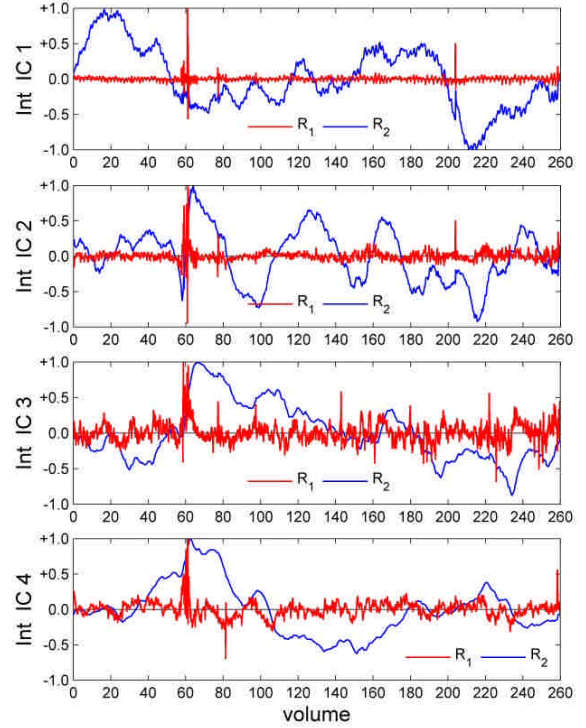


**Fig. 2.** Eight motion regressors obtained by integration of time courses of the four EEG independent components in Fig. 1. Temporal resolution is 4 ms. Tick labels along the time axis mark fMRI volumes acquired concurrently with EEG.

numbered 1 through 34 from bottom to top, and slices 2...33 are shown in Fig. 3. The distance between the central planes of adjacent EPI slices is 3.4 mm. The results in Fig. 3 demonstrate substantial improvements in tSNR after the application of E-REMCOR. The largest tSNR change is 112%, and a significant number of voxels show tSNR increases by 50% or more.

One interesting feature of the results in Fig. 3 is that the effects of E-REMCOR are significantly stronger for the even-numbered slices than for the odd-numbered slices. This is a consequence of the fact that the original fMRI data for Subject A exhibited reduced tSNR levels for the even-numbered slices compared to the odd-numbered slices. The reason for this is the following. During an interleaved EPI acquisition, the first half of the  $TR$  interval is used to acquire all odd-numbered slices, and the second half – to acquire all even-numbered slices. Because the largest through-plane motion occurred during the second half of the  $TR$  interval for volume 61 (Fig. 1), it affected the even-numbered slices, causing large fMRI signal variations and increasing standard deviations of the time courses. This effect is illustrated even further in Fig. 4, which compares time courses of two identical 12 mm diameter single-slice ROIs defined one above the other within two adjacent EPI slices in the frontal brain region. The results in Fig. 3 and Fig. 4 clearly demonstrate that large

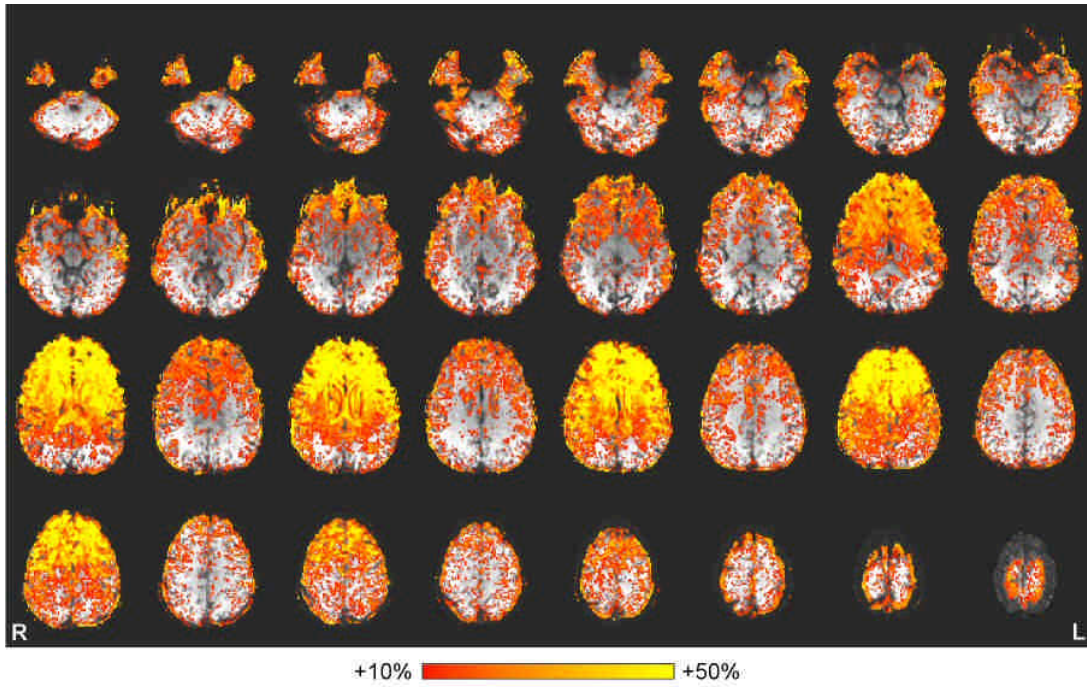


**Fig. 3.** Improvements in tSNR of single-subject fMRI data (Subject A) after the application of E-REMCOR with motion regressors exhibited in Fig. 2. The montage shows 32 axial EPI slices. The underlay image is a tSNR map for the original fMRI data (greyscale, display range 0–150), and the overlay (color) image is a map of the percent change in tSNR as a result of the E-REMCOR correction.

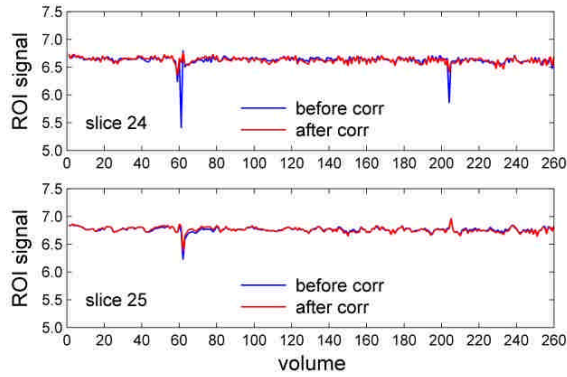


**Fig. 4.** Time courses of two 12 mm diameter single-slice ROIs, defined one above the other within two adjacent EPI slices, before and after the E-REMCOR procedure.

head motions occurring on time scales shorter than  $TR$  can have profound effects on fMRI time series, affecting different slices in different ways. Such motion effects can be efficiently reduced by application of E-REMCOR, which provides EEG-based motion regressors having high temporal resolution.

Figure 5 compares results of the E-REMCOR correction for the four subjects (A, B, C, and D). Four axial EPI slices with 10.2 mm spacing are shown for each subject. The lowest slice in each case is located approximately 10 mm above the superior edge of the anterior commissure. Figure 5 demonstrates that E-REMCOR visibly improves tSNR for all the subjects. Notably, all the images in Fig. 5 show tSNR

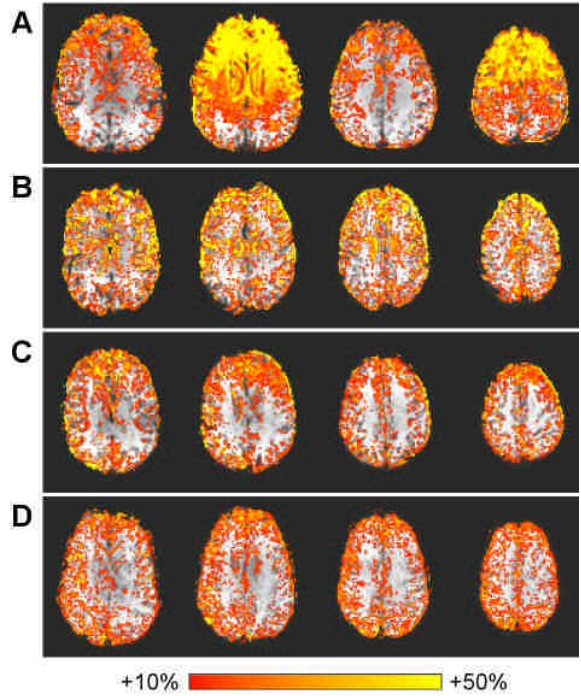


**Fig. 5.** Improvements in tSNR for four subjects after the application of E-REMCOR.

improvements for voxels near the edges of the brain, particularly in the frontal regions. fMRI time courses of such voxels are strongly affected by head motions due to partial volume effects.

Figure 6 provides an alternative measure of the

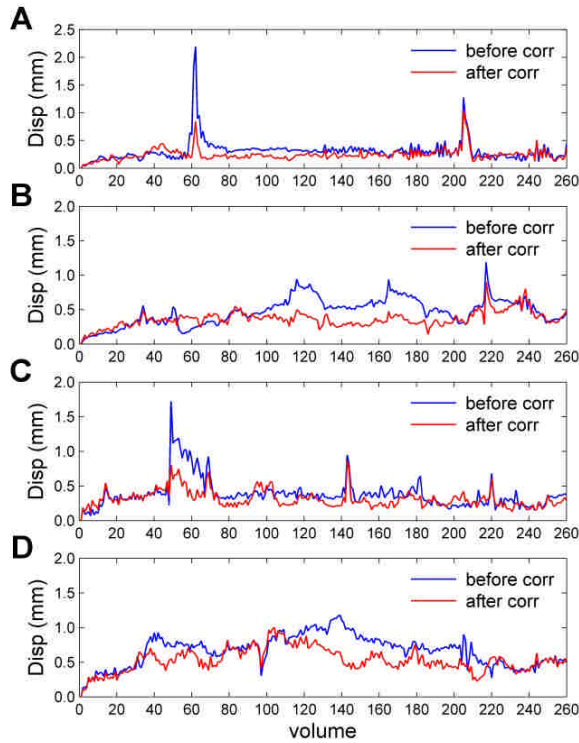


**Fig. 6.** The maximum displacements in brain automasks, estimated via the volume registration, for the fMRI datasets before and after the E-REMCOR procedure for four subjects. Linear de-trending was applied to the datasets prior to the volume registration.

motion correction efficiency. It exhibits the maximum displacement in the brain automask before and after the E-REMCOR procedure for each of the four subjects. This quantity was determined via volume registration of all 3D volumes in a given fMRI dataset with the first volume used as a reference. Both the original and corrected fMRI datasets were linearly de-trended before the volume registration to emphasize rapid and random head motions over slow and steady ones. Figure 6 indicates that the maximum displacement is reduced after the application of E-REMCOR for each of the four subjects. This reduction is particularly pronounced for the most drastic head movements exhibited by Subject A (volume 61) and Subject C (volume 49). In both cases, E-REMCOR reduced the maximum displacement by more than 50%. The six fMRI motion parameters (not shown) demonstrate a similar behavior: while their overall time courses do not change substantially as a result of the E-REMCOR procedure, their peak values, corresponding to drastic head motions, are reduced by as much as 50%. The average maximum displacements over the entire resting run before and after E-REMCOR for the four subjects are A) 0.31 mm and 0.24 mm; B) 0.47 mm and 0.36 mm; C) 0.38 mm and 0.31 mm; and D) 0.66 mm and 0.53 mm. The reduction in the average maximum displacement is thus around 20%. Therefore, the E-REMCOR procedure effectively reduces the

amount of head motion, as evaluated using the standard volume registration technique. While physical head motions remain the same, fMRI time courses for different voxels are corrected in such a way that a smaller effective displacement is needed to match a given fMRI volume to the reference volume.

Average results of the E-REMCOR correction for the four subjects are shown in Fig. 7 and Fig. 8. The map of percent changes in tSNR after the application of E-REMCOR for each subject was transformed to the Talairach space (Talairach and Tournoux, 1988) using that subject's high-resolution anatomical brain image. The four single-subject maps were re-sampled to  $2 \times 2 \times 2$  mm<sup>3</sup> isotropic voxel size, spatially smoothed using a Gaussian kernel with FWHM of 5 mm, and averaged. The axial slices in Fig. 7 have 3 mm spacing, with bottom/top slices corresponding to  $z = -27$  mm and  $z = 66$  mm, respectively, in the Talairach space. The largest tSNR improvement value in Figs. 7 and 8 is 31%, and many areas exhibit tSNR enhancements as high as 25%. Similar to the single-subject results in Fig. 5, the average results show significant tSNR increases near the surface of the brain, including the medial plane. The effects of E-REMCOR are most pronounced in the frontal brain areas, which typically exhibit the largest through-plane movements.

Figure 9 compares average results of the fMRI data correction by RETROICOR (Fig. 9a) and those after the simultaneous correction by E-REMCOR and RETROICOR (Fig. 9b). The linear regression procedure, Eq (9), included eight RETROICOR regressors (four cardiac and four respiratory) in the former case, and eight E-REMCOR regressors together with the eight RETROICOR regressors – in the latter case. The tSNR percent change maps were processed, averaged for the four subjects, and thresholded as described above for the results in Fig. 7. The axial slices in Fig. 9(a,b) have 5 mm spacing, with bottom/top slices corresponding to  $z = -20$  mm and  $z = 55$  mm, respectively, in the Talairach space. Comparison of the results in Fig. 9a and in Fig. 7 shows that E-REMCOR and RETROICOR complement each other: while E-REMCOR provides tSNR improvements in the frontal brain regions and near the brain edges, RETROICOR leads to tSNR enhancements in the areas close to blood vessels, such as sulci. Fig. 9b demonstrates that the simultaneous application of E-REMCOR and RETROICOR improves tSNR values across almost the entire brain by at least 10% over the original fMRI data. The maximum tSNR enhancement is 44% in Fig. 9b, compared to 28% in Fig. 9a. Overall tSNR improvements by as much as 35% are observed for many brain regions in Fig. 9b. Subtraction of the sum of the maps in Fig. 7 and Fig. 9a from the map in Fig. 9b shows additional tSNR increases by up to 6% due to the simultaneous regression, both in the regions affected by E-REMCOR and in those affected by RETROICOR.

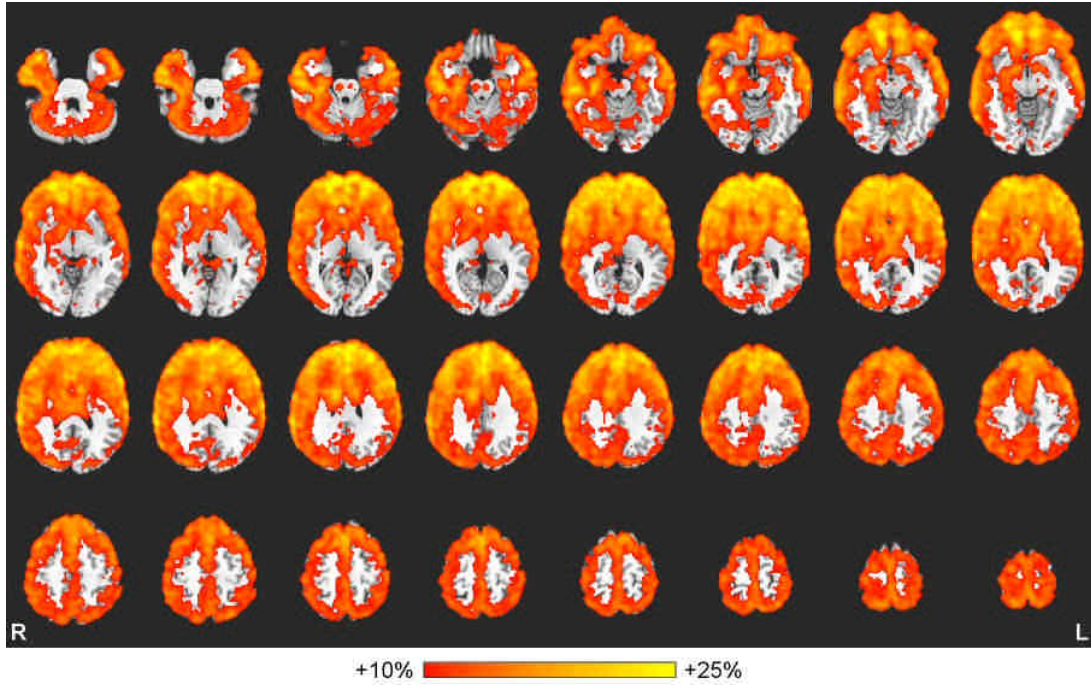


**Fig. 7.** Group results. Average improvement in tSNR for four subjects after the application of E-REMCOR. The results are projected onto the standard anatomical template (TT\_N27) in the Talairach space and shown with 3 mm spacing between the slices.

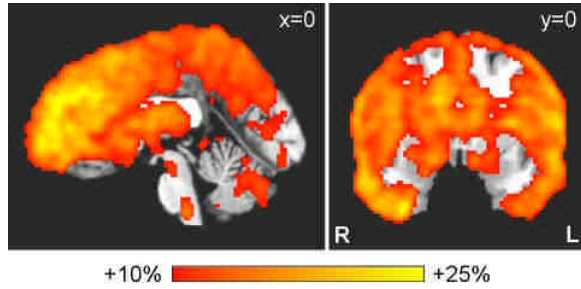


**Fig. 8.** Group results. Sagittal ( $x=0$  mm) and coronal ( $y=0$  mm) views of the data shown in Fig. 7.

The results in Fig. 9 demonstrate that the simultaneous application of E-REMCOR and RETROICOR is an efficient pre-processing step in fMRI data analysis. It should be followed by the volume registration with slice timing adjustment. Because the volume registration procedure also reduces variance in fMRI time courses, it is important to compare tSNR values for the datasets obtained by volume registration of the original (uncorrected) fMRI data and the data corrected by simultaneous E-REMCOR and RETROICOR. The results of such comparison are exhibited in Fig. 10. The correction was performed as explained above for Fig. 9b, and included eight E-REMCOR and eight RETROICOR regressors. The same volume registration procedure with slice timing adjustment was applied to both the original and the corrected datasets. The tSNR percent difference maps were processed, averaged, and displayed as described

above. Figure 10 shows significant widespread tSNR differences between the volume-registered versions of the corrected and uncorrected datasets, which are only slightly ( $<5\%$ ) lower than the tSNR differences between the corresponding datasets before the volume registration (Fig. 9b). Therefore, the simultaneous E-REMCOR and RETROICOR procedure has a pronounced effect on tSNR properties of fMRI time courses for subjects exhibiting large head movements, and this effect cannot be achieved or approximated using the volume registration procedure alone.

#### 4. Discussion

We have developed a novel EEG-assisted method for retrospective motion correction of fMRI data. E-REMCOR is capable of taking into account the effects of rapid rotational head motions, occurring on time scales shorter than  $TR$ . The reported results demonstrate the efficiency of E-REMCOR for fMRI motion correction by showing a) significant improvement in temporal SNR of fMRI time series; b) reduction in the apparent maximum displacement of brain images; and c) specificity of the correction effects to the brain regions most affected by head motions. In general, performance of E-REMCOR depends on how accurately the independent components describing random head movements are identified in the ICA decomposition of the EEG data. We consider this fact an advantage, because it encourages a careful examination of EEG artifacts, which would benefit the EEG-fMRI data

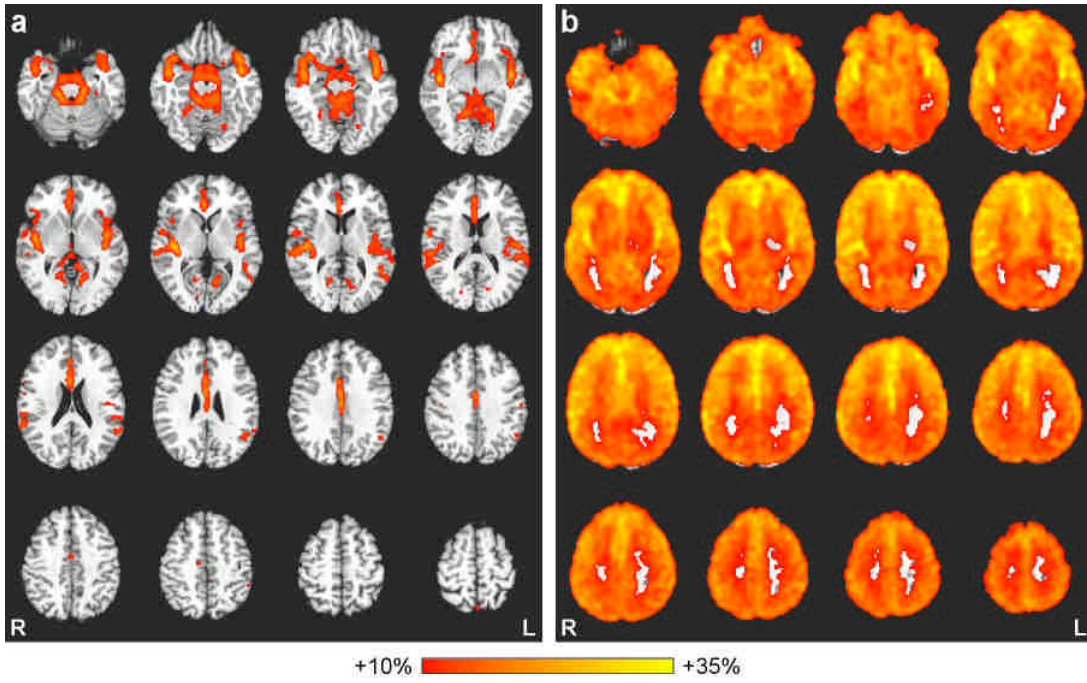


**Fig. 9.** Group results. a) Average improvement in tSNR for four subjects after the application of RETROICOR with 8 regressors. b) Average improvement in tSNR for four subjects after the simultaneous application of E-REMCOR (8 regressors) and RETROICOR (8 regressors). The results are shown in the Talairach space with 5 mm spacing between the slices.

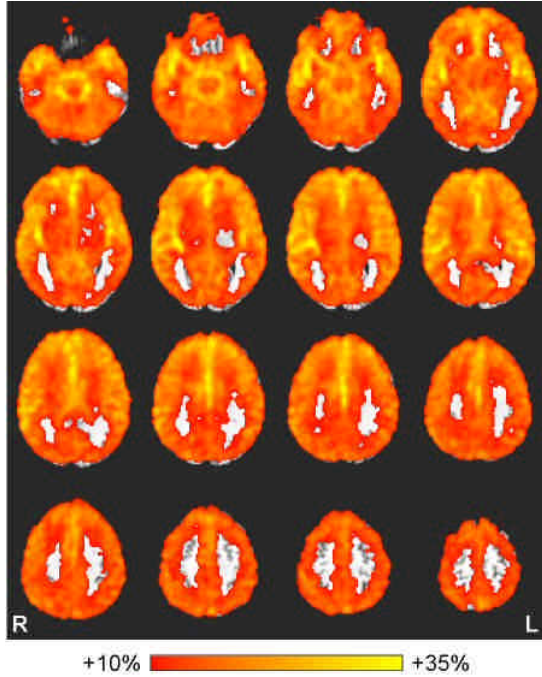


**Fig. 10.** Group results after volume registration. Average differences in tSNR between the volume-registered versions of the corrected (simultaneous E-REMCOR and RETROICOR) and of the original fMRI datasets for four subjects. The results are shown in the Talairach space with 5 mm spacing between the slices.

analysis in many ways.

An important property of E-REMCOR is that it can be applied simultaneously with RETROICOR and other

methods for physiological noise correction, as demonstrated in Fig. 9b. Such simultaneous regression improves the quality of both the random head motion correction by E-REMCOR and the physiological noise correction by RETROICOR, leading to average tSNR enhancements as high as 35% for large brain regions. This observation agrees with the conclusion, reached previously in the work by Jones et al., 2008, that motion correction improves RETROICOR performance. In principle, it is possible to use the ICs corresponding to cardioballistic artifacts in EEG data to generate regressors describing the small rigid-body head rotations due to cardiac activity. Such regressors can be somewhat redundant if RETROICOR is used at the same time. However, if random-motion and cardioballistic artifacts in EEG data are hard to separate, all motion-related ICs should be used to define E-REMCOR regressors.

It should be emphasized that E-REMCOR is not intended as a replacement for the traditional fMRI volume registration. Rather, it is a pre-processing method that should be applied to the original fMRI data with unaltered slice-time properties before the volume registration and slice timing correction. From this point of view, E-REMCOR is similar to RETROICOR. The purpose of this pre-processing step is to utilize the high temporal resolution of EEG to improve correction of the effects of rapid head movements that cannot be efficiently corrected by the volume registration procedure alone, as demonstrated by Fig. 10.

A limitation of E-REMCOR stems from the fact that

EEG motion artifacts are caused primarily by rotational head movements. Depending on the orientation of fMRI slices and the definition of the image reference frame, the artifacts will, in general, be functions of either three (pitch, roll, yaw) or two (pitch, roll) rotational motion parameters. The artifacts will not reflect translational head movements, if there are no deformations of the EEG array. This limitation, however, is not as serious as it might appear, because most head translations are accompanied by rotations in practice. The rotation-based motion regressors might be able to efficiently reduce the motion-related variance in fMRI time courses even in the absence of the translational regressors. For example, the most significant head motion, exhibited by Subject A (see Results section), included both rotational and translational movements. Yet, the E-REMCOR regressors, describing head rotations only, provided an efficient motion correction in this case.

As mentioned in Methods section, magnetic flux changes  $\Delta\Phi_b(t)$ , Eq (1), caused by deformations of the effective contours during head movements, generally depend on both rotational and translational motion parameters. The corresponding ICs (with topographies other than bipolar) can be identified in the ICA decomposition of the EEG data and used to generate regressors reflecting certain translational head movements. This approach, however, requires a better understanding of such deformational effects. Another interesting approach towards evaluation of general head motions by means of EEG involves a detailed analysis of the MRI artifacts in EEG recordings. Because the MRI artifacts are caused primarily by switching gradients, they incorporate information about both translational and rotational head movements.

The improved motion correction by E-REMCOR should be particularly beneficial for fMRI at 7 T, because stronger magnetic susceptibility artifacts at ultra-high fields make the motion effects more pronounced. It would also benefit the integration of fMRI with other neuroimaging modalities such as MEG (Zotev et al., 2008) and PET.

## 5. Conclusion

A novel EEG-based retrospective motion correction method for fMRI is presented. The main advantage of E-REMCOR is the ability to take into account the effects of rapid head motions, occurring on time scales shorter than  $TR$ . Because such motions affect only some of the slices within an fMRI volume, the resulting fMRI signal variations cannot be properly removed by volume registration or adequately described by the six fMRI motion parameters, determined from the volume registration. E-REMCOR takes advantage of the high temporal resolution of EEG to reduce the effects of rapid head movements in fMRI data, bridging the gap between

motion correction procedures in EEG and fMRI. E-REMCOR does not require any specialized equipment beyond the standard EEG-fMRI instrumentation and, importantly, can be applied retrospectively to any existing EEG-fMRI dataset. Application of E-REMCOR prior to fMRI volume registration can be expected to benefit fMRI data analysis for all subjects exhibiting significant head motions, including patients with neuropsychiatric disorders.

## Acknowledgments

This work was supported by the Laureate Institute for Brain Research and the William K. Warren Foundation. We would like to thank Dr. Robert Störmer, Dr. Patrick Britz, and Dr. Maria Schatt of Brain Products, GmbH for their continuous help and excellent technical support.

## References

- Allen, P.J., Polizzi, G., Krakow, K., Fish, D.R., Lemieux, L., 1998. Identification of EEG events in the MR scanner: the problem of pulse artifact and a method for its subtraction. *NeuroImage* 8, 229-239.
- Allen, P.J., Josephs, O., Turner, R., 2000. A method for removing imaging artifact from continuous EEG recorded during functional MRI. *NeuroImage* 12, 230-239.
- Bell, A.J., Sejnowski, T.J., 1995. An information-maximization approach to blind separation and blind deconvolution. *Neural Comput.* 7, 1129-1159.
- Bodurka, J., Ye, F., Petridou, N., Murphy, K., Bandettini, P.A., 2007. Mapping the MRI voxel volume in which thermal noise matches physiological noise – implications for fMRI. *NeuroImage* 34, 542-549.
- Bonmassar, G., Purdon, P.L., Jaaskelainen, I.P., Chiappa, K., Solo, V., Brown, E.N., Belliveau, J.W., 2002. Motion and ballistocardiogram artifact removal for interleaved recording of EEG and Eps during MRI. *NeuroImage* 16, 1127-1141.
- Cox, R.W., 1996. AFNI: software for analysis and visualization of functional magnetic resonance neuroimages. *Comput. Biomed. Res.* 29, 162-173.
- Cox, R.W., Hyde, J.S., 1997. Software tools for analysis and visualization of fMRI data. *NMR Biomed.* 10, 171-178.
- Cox, R.W., Jesmanowicz, A., 1999. Real-time 3D image registration for functional MRI. *Magn. Reson. Med.* 42, 1014-1018.
- Dumoulin, C.L., Souza, S.P., Darrow, R.D., 1993. Real-time position monitoring of invasive devices using magnetic resonance. *Magn. Reson. Med.* 29, 411-415.
- Friston, K.J., Ashburner, J., Frith, C.D., Poline, J.B., Heather, J.D., Frackowiak, R.S.J., 1995. Spatial registration and normalization of images. *Hum. Brain Mapping* 2, 165-189.
- Friston, K.J., Williams, S., Howard, R., Frackowiak, R.S.J., Turner, R., 1996. Movement-related effects in fMRI time-series. *Magn. Reson. Med.* 35, 346-355.
- Fu, Z.W., Wang, Y., Grimm, R.C., Rossman, P.J., Felmlee, J.P., Riederer, S.J., Ehman, R.L., 1995. Orbital navigator echoes for motion measurements in magnetic resonance imaging. *Magn. Reson. Med.* 34, 746-753.
- Glover, G.H., Li, T.Q., Ress, D., 2000. Image-based method for retrospective correction of physiological motion effects in fMRI: RETROICOR. *Magn. Reson. Med.* 44, 162-167.
- Hyvärinen, A., 1999. Fast and robust fixed-point algorithms for independent component analysis. *IEEE Trans. Neural Netw.* 10, 626-634.

- Hyvärinen, A., Oja, E., 2000. Independent component analysis: algorithms and applications. *Neural Netw.* 13, 411-430.
- Jansen, M., White, T.P., Mullinger, K.J., Liddle, E.B., Gowland, P.A., Francis, S.T., Bowtell, R., Liddle, P.F., 2012. Motion-related artefacts in EEG predict neuronally plausible patterns of activation in fMRI data. *NeuroImage* 59, 261-270.
- Jiang, A., Kennedy, D.N., Baker, J.R., Weisskoff, R.M., Tootell, R.B.H., Woods, R.P., Benson, R.R., Kwong, K.K., Brady, T.J., Rosen, B.R., Belliveau, J.W., 1995. Motion detection and correction in functional MR imaging. *Hum. Brain Mapping* 3, 224-235.
- Johnstone, T., Walsh, K.S.O., Greischar, L.L., Alexander, A.L., Fox, A.S., Davidson, R.J., Oakes, T.R., 2006. Motion correction and the use of motion covariates in multiple-subject fMRI analysis. *Hum. Brain Mapping* 27, 779-788.
- Jones, T.B., Bandettini, P.A., Birn, R.M., 2008. Integration of motion correction and physiological noise regression in fMRI. *Neuroimage* 42, 582-590.
- Makeig, S., Jung, T.P., Bell, A.J., Ghahremani, D., Sejnowski, T.J., 1997. Blind separation of auditory event-related brain responses into independent components. *Proc. Natl. Acad. Sci. USA* 94, 10979-10984.
- Mantini, D., Perrucci, M.G., Cugini, S., Ferretti, A., Romani, G.L., Del Gratta, C., 2007. Complete artifact removal for EEG recorded during continuous fMRI using independent component analysis. *NeuroImage* 34, 598-607.
- Masterton, R.A.J., Abbott, D.F., Fleming, S.W., Jackson, G.D., 2007. Measurement and reduction of motion and ballistogram artefacts from simultaneous EEG and fMRI recordings. *NeuroImage* 37, 202-211.
- Mulert, C., Lemieux, L., Eds., 2010. *EEG-fMRI: Physiological Basis, Technique, and Applications*. Springer-Verlag, Berlin Heidelberg.
- Nakamura, W., Anami, K., Mori, T., Saitoh, O., Cichocki, A., Amari, S.I., 2006. Removal of ballistocardiogram artifacts from simultaneously recorded EEG and fMRI data using independent component analysis. *IEEE Trans. Biomed. Eng.* 53, 1294-1308.
- Nunez, P.L., Srinivasan, R., 2006. *Electric Fields of the Brain: The Neurophysics of EEG*. Oxford University Press, Oxford New York.
- Ooi, M.B., Krueger, S., Muraskin, J., Thomas, W.J., Brown, T.R., 2011. Echo-planar imaging with prospective slice-by-slice motion correction using active markers. *Magn. Reson. Med.* 66, 73-81.
- Pruessmann, K.P., Weiger, M., Scheidegger, M.B., Boesiger, P., 1999. SENSE: sensitivity encoding for fast MRI. *Magn. Reson. Med.* 42, 952-962.
- Qin, L., van Gelderen, P., Derbyshire, J.A., Jin, F., de Zwart, J.A., Tao, Y., Duyn, J.H., 2009. Prospective head motion correction for high-resolution MRI using in-bore optical tracking system. *Magn. Reson. Med.* 63, 924-934.
- Talairach, J., Tournoux, P., 1988. *Co-Planar Stereotaxic Atlas of the Human Brain*. Thieme Medical Publishers, New York.
- Tremblay, M., Tam, F., Graham, S.J., 2005. Retrospective coregistration of functional magnetic resonance imaging data using external monitoring. *Magn. Reson. Med.* 53, 141-149.
- Ward, H.A., Riederer, S.J., Grimm, R.C., Ehman, R.L., Felmlee, J.P., Jack, C.R., Jr., 2000. Prospective multiaxial motion correction for fMRI. *Magn. Reson. Med.* 43, 459-469.
- Welch, E.B., Manduca, A., Grimm, R.C., Ward, H.A., Jack Jr., C.R., 2002. Spherical navigator echoes for full 3D rigid body motion measurement in MRI. *Magn. Reson. Med.* 47, 32-41.
- Yan, W.X., Mullinger, K.J., Geirsdottir, G.B., Bowtell, R., 2010. Physical modeling of pulse artefact sources in simultaneous EEG/fMRI. *Hum. Brain Mapp.* 31, 604-620.
- Zaitsev, M., Dold, C., Sakas, G., Hennig, J., Speck, O., 2006. Magnetic resonance imaging of freely moving objects: prospective real-time motion correction using an external optical motion tracking system. *NeuroImage* 31, 1038-1050.
- Zotev, V.S., Matlashov, A.N., Volegov, P.L., Savukov, I.M., Espy, M.A., Mosher, J.C., Gomez, J.J., Kraus, R.H., 2008. Microtesla MRI of the human brain combined with MEG. *J. Magn. Reson.* 194, 115-120.
- Zotev, V., Krueger, F., Phillips, R., Alvarez, R.P., Simmons, W.K., Bellgowan, P., Drevets, W.C., Bodurka, J., 2011. Self-regulation of amygdala activation using real-time fMRI neurofeedback. *PLoS ONE* 6, e24522 (1-17).